

Dummy Molecularly Imprinted Polymers for Analyzing Fluorene and Phenanthrene: An Integrative Study of Adsorption Isotherms, Kinetics, and Thermodynamics

Aria Pinandita¹, Nurrahmi Handayani^{2,3}, Muhammad Iqbal², Untung Triadhi², Rusnadi Rusnadi^{2,3}, Samitha Dewi Djajanti², Muhammad Bachri Amran², and Muhammad Ali Zulfikar^{2,3*}

¹Doctoral Program of Chemistry, Faculty of Mathematics and Natural Sciences, Institut Teknologi Bandung, Jl. Ganesha No. 10, Bandung 40132, Indonesia

²Division of Analytical Chemistry, Faculty of Mathematics and Natural Sciences, Institut Teknologi Bandung, Jl. Ganesha No. 10, Bandung 40132, Indonesia

³Research Center for Nanosciences and Nanotechnology, Institut Teknologi Bandung, Jl. Ganesha No. 10, Bandung 40132, Indonesia

* **Corresponding author:**

email: zulfikar@itb.ac.id

Received: August 10, 2025

Accepted: December 1, 2025

DOI: 10.22146/ijc.110267

Abstract: A dummy molecularly imprinted polymer was synthesized using anthrone as a dummy template, styrene as the functional monomer, ethylene glycol dimethacrylate as the crosslinker, and benzoyl peroxide as the initiator for the selective adsorption of fluorene and phenanthrene. The interactions between anthrone and styrene were evaluated by UV-vis titration and Job's plot to determine the optimal binding stoichiometry. FTIR, TGA, SEM and BET-BJH analyses confirmed effective template removal and the formation of recognition cavities. Isotherm studies showed that fluorene adsorption followed the Langmuir model ($R^2 = 0.9988$), with a maximum adsorption capacity of 12.221 mg g^{-1} and a Langmuir constant of 5.293 L mg^{-1} . In contrast, the Freundlich model best described the adsorption of phenanthrene ($R^2 = 0.9997$), yielding a Freundlich constant of $24.463 (\text{mg g}^{-1})(\text{L mg}^{-1})^{1/n}$ and a $1/n$ value of 0.288. Kinetic analysis revealed pseudo-second-order model behavior ($R^2 > 0.99$), with rate constants of $0.261 \text{ g mg}^{-1} \text{ min}^{-1}$ for phenanthrene and $0.0059 \text{ g mg}^{-1} \text{ min}^{-1}$ for fluorene. Thermodynamic evaluations indicated that phenanthrene adsorption was enthalpy-driven and exothermic, whereas fluorene adsorption was entropy-driven and endothermic. Both adsorption processes were spontaneous, confirming the potential of the anthrone-based dummy molecularly imprinted polymer as an efficient sorbent for polycyclic aromatic hydrocarbons.

Keywords: dummy molecularly imprinted polymer; anthrone; fluorene; phenanthrene; adsorption

■ INTRODUCTION

Polycyclic aromatic hydrocarbons (PAHs) such as fluorene and phenanthrene are recognized as persistent organic pollutants that are widely distributed in aquatic environments due to industrial activities, incomplete combustion, and hydrocarbon waste discharge [1-3]. Their hydrophobicity and toxicity have been associated with bioaccumulation in sediments and food chains, posing serious risks to ecosystems and human health [4-6]. Therefore, selective, sensitive, and environmentally

friendly analytical methods are urgently required for the detection and monitoring of PAHs [7-9].

An emerging approach involves the use of dummy molecularly imprinted polymers (DIPs), which are synthesized using structural analogs of the target analytes [10]. By avoiding the direct use of the actual PAH compounds during polymer preparation, the risk of target contamination is eliminated [11-13]. This strategy enhances selectivity and safety while also aligning with the principles of green chemistry by

minimizing the use of hazardous compounds and reducing the generation of toxic waste [14-15].

To ensure that the functional monomer and dummy template exhibit appropriate interactions prior to polymer synthesis, experimental spectroscopic approaches were employed. UV-vis titration methods, including the Benesi–Hildebrand analysis, Job's plot, and the Hill equation, were used to evaluate binding interactions and determine the stoichiometry of the pre-polymerization complexes [16]. These experimental techniques provided essential information for selecting suitable monomer–template ratios and optimizing the formation of recognition sites in the resulting polymers.

Following these preliminary evaluations, the DIP was synthesized using the selected monomer–template system. Its performance was assessed through adsorption studies, including adsorption isotherms, adsorption kinetics, and thermodynamic analyses, to elucidate the adsorption mechanism and quantify the affinity of the polymer toward fluorene and phenanthrene [17-19]. These evaluations helped determine the adsorption capacities, rate constants, and thermodynamic parameters associated with the binding process. This integrated experimental approach offers mechanistic insights into the adsorption behavior of PAHs while supporting the rational and sustainable design of polymeric adsorbents. By combining detailed spectroscopic evaluation of monomer–template interactions with comprehensive adsorption studies, the present work aims to contribute to the development of selective, efficient, and environmentally friendly materials for aquatic environmental monitoring.

■ EXPERIMENTAL SECTION

Materials

All reagents and solvents used in this study were of analytical or HPLC grade and were obtained from Merck (Germany). Anthrone was used as a dummy template, while styrene served as the functional monomer. Ethylene glycol dimethacrylate (EGDMA) was used as the crosslinking agent, and benzoyl peroxide (BPO) was used as the radical initiator. Acetonitrile was used both as a porogenic solvent in the polymerization process and as

the mobile phase in HPLC analysis. Fluorene and phenanthrene were used as target analytes in adsorption studies. Ultrapure water was used in all aqueous preparations and adsorption experiments.

Instrumentation

Material characterization was performed to evaluate the structural, morphological, and physicochemical properties of the synthesized DIP and NIP polymers. Fourier-transform infrared (FTIR) spectroscopy was carried out using a Shimadzu Prestige 21 spectrometer to identify functional groups. Surface morphology was examined using scanning electron microscopy (SEM) with a Hitachi SU 3500, while the specific surface area and pore structure were determined using the Brunauer–Emmett–Teller (BET) and BJH methods on a NOVA–Quantachrome Instruments version 10.01. Thermal stability was assessed using thermogravimetric analysis (TGA) with a NETZSCH STA 449 F1 instrument. All characterizations were conducted after the template-removal (leaching) process, with the non-imprinted polymer (NIP) serving as a reference.

To evaluate monomer–template interactions prior to polymer synthesis, UV-vis measurements were conducted using a double-beam UV-vis spectrophotometer. Spectroscopic analyses included Benesi–Hildebrand plots, Job's method of continuous variation, and Hill equation analysis to estimate binding stoichiometry and interaction strength. These methods enabled the identification of optimal experimental conditions for polymer imprinting.

All adsorption experiments, including isotherm, kinetics, and thermodynamics studies, were analyzed using high-performance liquid chromatography (HPLC) equipped with a C-18 column (Fortis UniverSil, 5 μm particle size, 30 cm \times 250 \times 4.6 mm). The mobile phase consisted of acetonitrile–water (70:30, v/v), delivered at a flow rate of 1.0 mL/min, with an injection volume of 100 μL . Detection was carried out at a wavelength of 254 nm. This chromatographic method enabled accurate determination of equilibrium concentrations for adsorption isotherm analysis, time-dependent concentrations for kinetic modelling, and temperature-dependent equilibrium concentrations for

thermodynamic evaluation. The accuracy of this approach ensured consistency across the different adsorption analysis.

Procedure

UV-vis titration study

To examine the interaction between the dummy template (anthrone), target analytes (fluorene and phenanthrene), and the functional monomer (styrene), UV-vis titration experiments were conducted under controlled conditions. These experiments were designed to determine the binding constants and stoichiometry of the pre-polymerization complexes, providing insight into the molecular interactions governing imprinting efficiency.

The target analytes (fluorene and phenanthrene) as well as the dummy template (anthrone) were titrated with the chosen functional monomer (styrene) under controlled conditions. Specifically, 5 mL of fluorene solution (2 ppm) was titrated with incremental additions of styrene solution (20 ppm), 5 mL of phenanthrene solution (1 ppm) was titrated with styrene solution (20 ppm), and 5 mL of anthrone solution (2 ppm) was titrated with styrene solution (40 ppm).

The concentrations of the titrants were selected to ensure that the absorbance values of the resulting complexes remained within the optimal range of 0.2–0.8, with a target central absorbance of approximately 0.4, thereby minimizing photometric error. Absorbance measurements were carried out after each addition, and all absorbance values were corrected for dilution effects caused by the incremental titration volumes before further analysis.

The corrected absorbance data were analyzed using three complementary methods. The Benesi–Hildebrand method was applied to calculate the association constant (K_{assoc}) for 1:1 complex formation according to the following equation [16], where C_{monomer} is the monomer concentration expressed in mol/L, as shown in Eq. (1).

$$\frac{1}{\Delta A} = \frac{1}{\Delta \epsilon} + \frac{1}{K_{\text{assoc}} \times \Delta \epsilon \times C_{\text{monomer}}} \quad (1)$$

Job's method of continuous variations was used to determine the stoichiometry of the complexes. The absorbance of the complex multiplied by the mole

fraction of the template molecules was plotted against the mole fraction of the monomer, and the peak of the resulting curve indicated the most probable stoichiometric ratio.

The Hill equation was further used to evaluate cooperative binding behavior and confirm the binding constant [16], where the parameter n represents the degree of cooperativity in the binding process between the functional monomer and the template/dummy molecules, as shown in Eq. (2).

$$\Delta A = \frac{\Delta A_{\text{max}} \times K_{\text{assoc}} \times C_{\text{monomer}}}{1 + K_{\text{assoc}} \times C_{\text{monomer}}} \quad (2)$$

Finally, the experimental values of K_{assoc} were converted into binding free energies (ΔG) using the thermodynamic relationship, where R is the universal gas constant ($1.987 \text{ cal mol}^{-1} \text{ K}^{-1}$), as shown in Eq. (3):

$$\Delta G = -RT \ln K_{\text{assoc}} \quad (3)$$

These ΔG values were then compared with the binding free energies obtained from the adsorption thermodynamics study. This comparison was based on the assumption that UV-vis titration between the monomer and either the target analytes or the dummy template provides a preliminary estimation of interaction strength. Thus, the UV-vis-derived association parameters offer a fundamental reference for evaluating the thermodynamic results and for determining the appropriate monomer-to-template composition in the synthesis of dummy molecularly imprinted polymers.

Synthesis of DIP and NIP

DIP was synthesized using the precipitation polymerization method. In a 100 mL glass reaction vessel, 0.5 mmol of anthrone, 1 mmol of styrene, and 20 mmol of ethylene glycol dimethacrylate were dissolved in 50 mL of acetonitrile. After complete dissolution, 250 mg of benzoyl peroxide was added. The resulting solution was purged with nitrogen gas for 10 min to remove dissolved oxygen, and then sealed and heated in an oven at $80 \text{ }^\circ\text{C}$ for 2 h to initiate and complete polymerization. After cooling to room temperature, the resulting polymer was collected and sieved to isolate particles in the desired size range (passing through 60 mesh and retained on 80 mesh). The

NIP was synthesized using the same procedure without the addition of the dummy template and was used as a control in all comparative studies.

Elimination of template molecule from synthesized polymers

The template molecule was removed by a leaching process using acetonitrile. In each leaching cycle, 200 mg of the polymer was suspended in 10 mL of fresh acetonitrile and sonicated for 10 min. The process was repeated with fresh solvent until no detectable absorbance of anthrone was observed using UV-vis spectrophotometry, confirming the complete removal of the template molecule.

Adsorption capability and models experiments

Stock solutions of fluorene and phenanthrene at a concentration of 1000 ppm were prepared in acetonitrile. Each 10 mg of fluorene and/or phenanthrene was accurately weighed using an analytical balance and transferred into a 10 mL volumetric flask. A small amount of acetonitrile was added to each flask to dissolve the compounds. After complete dissolution, the solutions were diluted to the 10 mL mark with acetonitrile. The resulting stock solutions were stored in amber bottles, tightly closed, and protected from light to prevent degradation.

For adsorption experiments, aqueous test solutions with concentrations ranging from 0.4 to 1.4 ppm were prepared by diluting the stock solutions with deionized water. The required volume of the 1000 ppm stock solution was pipetted using a micropipette and transferred into a 500 mL volumetric flask. Depending on the desired final concentration, volumes between 200 μ L (for 0.4 ppm) and 700 μ L (for 1.4 ppm) were used. After pipetting the stock solution, deionized water was added to reach the 500 mL mark. The flasks were then shaken several times to ensure homogeneity before use.

Adsorption isotherm experiments were conducted to evaluate the adsorption capacities and isotherm models of DIP and NIP sorbents for fluorene and phenanthrene. A total of 10 mg of each sorbent, DIP and NIP was added to 200 mL of aqueous test solutions containing either fluorene or phenanthrene at varying concentrations. For fluorene, the concentration range was 0.4 to 1.4 ppm,

while for phenanthrene the range was 0.4 to 1.2 ppm. The mixtures were placed in sealed glass containers and allowed to equilibrate at room temperature for 2 h under gentle shaking. After the contact period, the sorbents were separated from the solution by filtration or centrifugation. The residual concentration of the analytes in the supernatant was analyzed using high-performance liquid chromatography to determine the amount of analyte adsorbed onto the sorbent. The adsorption capacity (q_e , mg/g) at equilibrium was calculated based on the difference between the initial (C_{initial} , ppm) and final concentrations (C_e , ppm), as shown in Eq. (4). This procedure was conducted in triplicate to ensure reproducibility, and all glassware was cleaned thoroughly to avoid contamination.

$$q_e = \frac{(C_{\text{initial}} - C_e) \times \text{volume}}{\text{mass}} \quad (4)$$

The adsorption capacity data obtained from DIP and NIP were subsequently fitted to three linearized isotherm models: the Langmuir model, the Freundlich model, and the Temkin model, corresponding to Eq. (5–7), respectively. This fitting process was carried out to determine the most suitable adsorption isotherm for describing the interaction between the sorbents and the target analytes, as well as to estimate the relevant adsorption parameters [17–19].

$$\frac{1}{q_e} = \frac{1}{q_{\text{max}} \times K_L \times C_e} + \frac{1}{q_{\text{max}}} \quad (5)$$

$$\log q_e = \log K_F + \frac{1}{n} \log C_e \quad (6)$$

$$q_e = B \ln A + B \ln C_e \quad (7)$$

Adsorption kinetics study

The adsorption kinetics of the synthesized DIP and the corresponding NIP were investigated using fluorene and phenanthrene as model analytes. A total of 10 mg of each sorbent was added to 200 mL of aqueous solution containing 1 ppm fluorene and 1 ppm phenanthrene. The mixtures were agitated in a thermostatic shaker at a constant temperature (298 K) and fixed stirring rate (100 rpm) to ensure homogeneous suspension. Aliquots were withdrawn at predetermined time intervals (15, 30, 45, 60, 75, 90, 105, and 120 min), immediately filtered through a 0.22 μ m syringe filter, and analyzed to

determine the residual concentrations of fluorene and phenanthrene. The kinetic data were fitted to two commonly used models: the pseudo-first-order (PFO) model, as shown in Eq. (8) and the pseudo-second-order (PSO) model [20] as shown in Eq. (9), where q_e and q_t represent the amounts of adsorbate adsorbed at equilibrium and at time t (mg/g), respectively [17-19].

$$\ln(q_e - q_t) = \ln q_e - k_1 t \quad (8)$$

$$\frac{t}{q_t} = \frac{1}{k_2 q_e^2} + \frac{t}{q_e} \quad (9)$$

Adsorption thermodynamics study

The thermodynamic parameters of fluorene and phenanthrene adsorption onto the DIP and NIP were investigated at three different temperatures (298, 313, and 333 K, corresponding to 25, 40, and 60 °C). For each experiment, 10 mg of sorbent was added to 200 mL of aqueous solution with varying initial concentrations ranging from 0.4 to 1.4 ppm for fluorene and 0.4 to 1.2 ppm for phenanthrene. The mixtures were equilibrated under constant agitation until adsorption equilibrium was reached, and the residual concentrations of the analytes were determined by HPLC.

For thermodynamic analysis, the Langmuir constant was converted from L/mg to L/mol using the molar mass (g/mol) of the analyte. By plotting $\ln K$ against $1/T$ (van't Hoff equation), ΔH was obtained from the slope and ΔS from the intercept [17], as shown in Eq. (10).

$$\ln K_L = -\frac{\Delta H}{RT} + \frac{\Delta S}{R} \quad (10)$$

To strengthen the reliability of the thermodynamic interpretation, the ΔG values obtained from Langmuir isotherm fitting were directly compared with those calculated from UV-vis titration data using the Benesi-Hildebrand method and the Hill equation. These UV-vis-derived ΔG values were determined from the association constants obtained for the interactions between the monomer and each target analyte or dummy template. In addition, the material's thermal stability, as evaluated by TGA, was considered to support the overall feasibility of the adsorption process. This comparative approach ensured consistency between spectroscopically derived interaction parameters and the experimentally observed adsorption behavior.

RESULTS AND DISCUSSION

The molecular structures of fluorene, phenanthrene, and anthrone were compared to rationalize the selection of anthrone as a dummy template in the synthesis of the molecularly imprinted polymer, as shown in Fig. 1. Fluorene and phenanthrene are representative low molecular weight PAHs, both consisting of fused aromatic rings that contribute to their hydrophobicity and persistence in aquatic environments [1-3]. Anthrone can be described as an oxidized derivative of anthracene, sharing a comparable polycyclic aromatic backbone while being less toxic, thereby representing a safer dummy template. Moreover, its molecular weight is similar to that of low molecular weight PAHs, reinforcing its structural analogy.

A key feature of anthrone and fluorene is the presence of sp^3 -hybridized carbons in their frameworks, which slightly disrupts planarity and increases the flexibility of the binding cavities once imprinted. This contrasts with phenanthrene, which is fully aromatic and structurally rigid. The flexibility imparted by sp^3 carbons is advantageous for rebinding in aqueous conditions, where a degree of conformational adaptability enhances recognition efficiency.

UV-vis binding analyses based on the Benesi-Hildebrand and Hill methods (Tables 1 and 2). The ΔG values obtained with the Benesi-Hildebrand approach (-5.52 to -6.07 kcal/mol) indicated moderate 1:1 binding affinity between styrene and the analytes/templates. In contrast, the ΔG values determined using the Hill method (-11.71 to -13.98 kcal/mol) reflected substantially stronger cooperative interactions, suggesting that the binding process favored the participation of more than one monomer molecule. The Hill parameter n for the anthrone-styrene system was 1.92, indicating that the 1:2

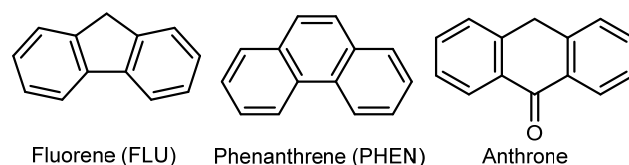


Fig 1. Chemical structures of fluorene, phenanthrene, and anthrone

Table 1. ΔG determination using the Benesi–Hildebrand method

Parameters	Anthrone	Fluorene	Phenanthrene
Slope	2.9658×10^{-5}	4.4999×10^{-5}	2.2344×10^{-5}
Intercept	0.7859	1.1811	1.5979
K	26497.9211	26246.9419	71511.5785
R ²	0.9931	0.9859	0.9815
ln K	10.1848	10.1753	11.1776
ΔG (kcal/mol)	-5.5280	-5.5230	-6.0670
$\Delta \epsilon$	1.2720	0.8470	0.6260

Table 2. ΔG determination using the Hill method

Parameters	Anthrone	Fluorene	Phenanthrene
ΔA_{\max}	0.5628	0.4009	0.2982
ln K	22.4302	21.5825	25.7492
n	1.9228	1.8574	2.0350
R ²	0.9880	0.9995	0.9932
ΔG (kcal/mol)	-12.1740	-11.7140	-13.9750

complex was thermodynamically more favorable and more stable than the 1:1 complex.

The UV-vis titration results (Fig. 2) further supported this conclusion. The Job's plot exhibited a distinct maximum at a mole fraction of approximately 0.66, consistent with the formation of a dominant 1:2 anthrone–styrene complex. This observation aligns with the Hill analysis, where the cooperativity factor approached 2, and confirms that the 1:2 stoichiometry

provides stronger and more energetically favorable binding than the 1:1 configuration. The convergence of the Benesi–Hildebrand, Hill, and Job's plot analyses thus consistently identified the 1:2 complex as the preferred and most stable species in solution. Accordingly, this ratio was selected for the synthesis of the DIP, ensuring optimal template interaction and enhanced selective binding toward the target analytes.

The FTIR spectra (Fig. 3) confirmed the presence of functional groups from styrene, EGDMA, and the dummy template anthrone. A strong band at 1720–1730 cm^{-1} corresponded to C=O stretching of EGDMA, while aromatic C=C stretches (1600–1450 cm^{-1}) and C–H out-of-plane bending (750–700 cm^{-1}) verified aromatic ring incorporation from styrene and anthrone. Aliphatic C–H stretching (2950–2850 cm^{-1}) and C–O stretching (1250–1150 cm^{-1}) reflected styrene and EGDMA contributions [20]. Before leaching, DIP spectra displayed additional anthrone-specific peaks (1672, 1593, and 1507 cm^{-1} ; 840 and 757 cm^{-1}), which diminished or disappeared after leaching, indicating effective template removal. Due to overlapping signals with styrene and EGDMA, TGA analysis was employed to further validate these findings.

TGA–DTG analysis was used to assess the thermal stability and leaching efficiency of DIP, as shown in Fig. 4. Before leaching, DIP exhibited two degradation stages:

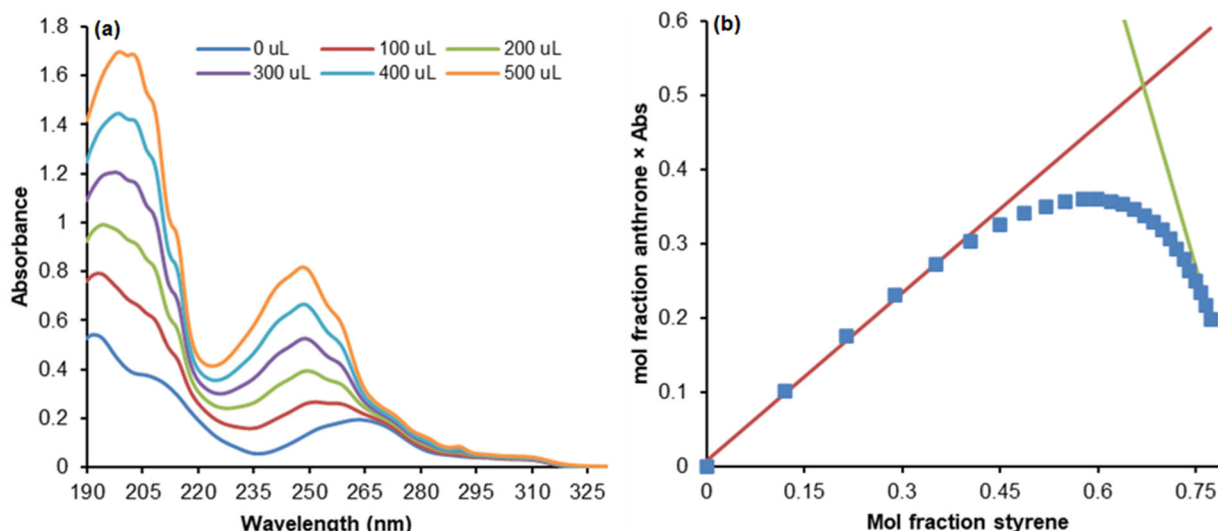


Fig 2. (a) UV-vis titration spectrum of anthrone (2 ppm, 5 mL) with styrene (40 ppm) and (b) the corresponding Job's plot

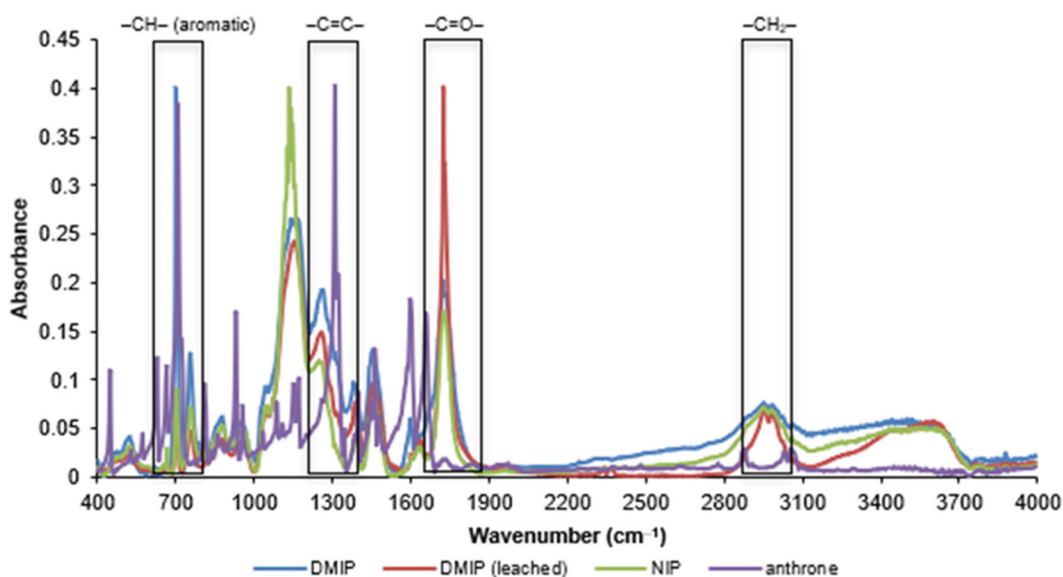


Fig 3. FTIR spectra of anthrone, NIP, DIP before leaching, and DIP after leaching

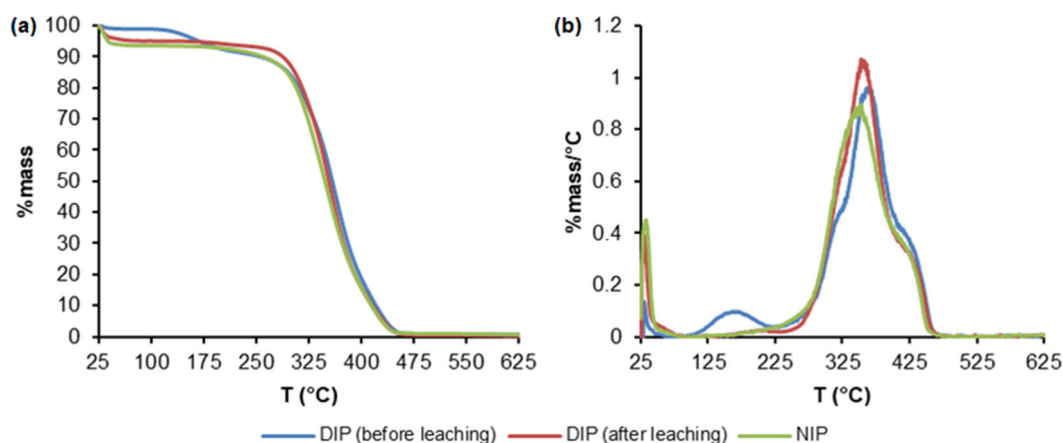


Fig 4. (a) TGA and (b) DTG profiles of NIP, DIP before leaching, and DIP after leaching

an early DTG peak at 161.9 °C, attributed to residual anthrone (close to its melting point, 154.0–157.0 °C), and a second peak at 365.5 °C, corresponding to polymer backbone decomposition. After leaching, only a single degradation peak at 352.4 °C remained, confirming anthrone removal and yielding a profile similar to NIP (353.4 °C). The disappearance of the anthrone-related peak indicates successful cavity formation, later supported by SEM and BET analyses that confirmed increased porosity and surface area.

SEM analysis revealed notable morphological differences between DIP and NIP. Both polymers formed nearly spherical particles; however, DIP showed a rougher surface with irregular textures and partially fused particles

(Fig. 5). DIP displayed visible imprint cavities formed after the removal of anthrone, while NIP appeared smooth and uniform without such cavities, confirming the absence of specific recognition sites. BET analysis further supported these observations, with DIP exhibiting a markedly higher specific surface area (16.243 m²/g) than NIP (0.074 m²/g), consistent with the formation of mesoporous structures.

These results (Table 3) confirm that template removal successfully generated porous DIP particles with enhanced potential for selective adsorption. These morphological and surface area differences strongly suggest the formation of functional recognition cavities in DIP, which are expected to influence its adsorption

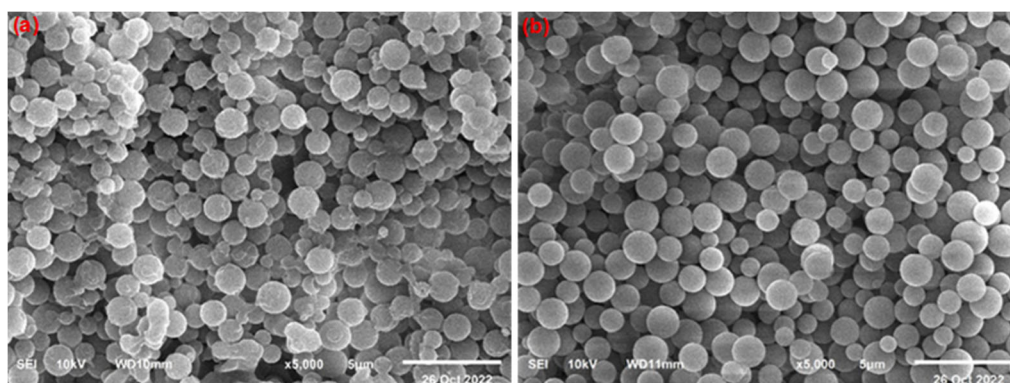


Fig 5. SEM Micrographs of DIP (a) and NIP (b) at 5000 \times magnification

Table 3. BET specific surface area and BJH desorption pore radius of DIP and NIP

Sorbent	BET specific surface area	BJH pore radii
DIP	16.243 m ² /g	18.995 nm
NIP	0.074 m ² /g	17.032 nm

performance. To verify this, adsorption isotherm studies were subsequently carried out to provide quantitative insight into the binding characteristics of the imprinted sites.

The adsorption performance of the DIP was compared with that of the NIP using isotherm models, as shown in Table 4. Higher K_L and q_{max} on DIP confirmed stronger and more specific binding for both analytes, with phenanthrene showing the highest affinity ($q_{max} =$

16.484 mg/g, $K = 47.380$ L/mg). Imprinting factors, calculated as the ratio of q_{max} for MIP to q_{max} for NIP, yielded values of 1.16 (fluorene) and 1.09 (phenanthrene) indicating moderate imprinting efficiency. Freundlich $1/n$ values suggested greater surface heterogeneity on DIP, particularly for phenanthrene ($1/n = 0.288$), while Temkin analysis revealed more favorable sorbate-sorbate interactions on DIP, consistent with better analyte orientation in the recognition sites. The stronger affinity of DIP toward phenanthrene was attributed to its planar three-ring structure, which promotes efficient π - π stacking within the styrene-based matrix. In contrast, the bent conformation of fluorene, due to its $C-sp^3$ bridgehead, limited such interactions. Model fitting showed that fluorene adsorption followed the

Table 4. Adsorption isotherm models for DIP and NIP with fluorene (FLU) and phenanthrene (PHEN)

Isotherm models	Parameter	NIP-FLU	DIP-FLU	NIP-PHEN	DIP-PHEN
Langmuir	Slope	0.0213	0.0155	0.0021	0.0013
	Intercept	0.0946	0.0818	0.0660	0.0607
	R ²	0.9993	0.9988	0.9680	0.9430
	q_{max} (mg/g)	10.5760	12.2210	15.1530	16.4840
	K (L/mg)	4.4410	5.2930	30.8860	47.3800
Freundlich	Slope	0.3620	0.3591	0.2715	0.2881
	Intercept	0.9564	1.0428	1.2903	1.3885
	R ²	0.9739	0.9765	0.9947	0.9997
	K (mg/g)(L/mg) ^{1/n}	9.0440	11.0350	19.5100	24.4630
	1/n	0.3620	0.3590	0.2720	0.2880
Temkin	Slope	2.3317	2.6905	2.9425	3.4066
	Intercept	8.7938	10.6099	17.5957	20.9675
	R ²	0.9919	0.9940	0.9976	0.9856
	ln A	3.7710	3.9430	5.9800	6.1550
	B	2.3320	2.6900	2.9420	3.4070

Langmuir model (monolayer, $R^2 = 0.9988$), while phenanthrene on DIP fit best with the Freundlich model (multilayer on a heterogeneous surface, $R^2 = 0.9997$). Temkin model fitting also indicated good correlation for both analytes ($R^2 = 0.9940$ for fluorene, 0.9856 for phenanthrene). These findings confirmed that imprinting improved binding affinity and specificity, particularly for phenanthrene.

The adsorption kinetic data (Table 5) were analyzed using both the PFO and PSO models. The PSO model exhibited superior fitting performance, as reflected in the higher correlation coefficients ($R^2 = 0.998$ – 0.999) compared to the PFO model ($R^2 = 0.711$ – 0.979), indicating that adsorption was governed primarily by site-specific interactions rather than simple physical adsorption. Interestingly, the adsorption rate constants (k_2) for the DIP were lower than those of the NIP. This reduction is attributed to the need for conformational adjustment of the imprinted cavities in DIP, which slows the initial adsorption process. In contrast, the NIP allows rapid nonspecific physical adsorption, albeit with lower q_e . Despite this trade-off, DIP achieved higher q_e values,

demonstrating that dummy molecular imprinting enhanced binding specificity.

A notable difference was observed between the two analytes. Phenanthrene exhibited a faster adsorption rate than fluorene in both polymers. This can be explained by the propensity of phenanthrene molecules to form stable π - π stacked dimers within the imprinted cavities. The fully planar conjugated structure of phenanthrene facilitates face-to-face stacking interactions, which are energetically favorable and further stabilize the adsorption process. In contrast, fluorene, due to the presence of a C- sp^3 bridgehead carbon that disrupts planarity, has a diminished ability to form such stable π - π stacked dimers. Consequently, its adsorption relies more on weaker van der Waals interactions or hydrophobic effects, resulting in slower kinetics compared to phenanthrene.

The thermodynamic parameters of fluorene and phenanthrene adsorption onto DIP are summarized in Table 6 and illustrated by the van't Hoff plot in Fig. 6. The adsorption of phenanthrene was exothermic, as indicated by the negative enthalpy change ($\Delta H = -16.12$ kcal/mol), whereas fluorene adsorption was endothermic,

Table 5. Pseudo-first-order (PFO) and pseudo-second-order (PSO) adsorption kinetic models applied to DIP and NIP for fluorene (FLU) and phenanthrene (PHEN)

Kinetic	Parameter	NIP-FLU	DIP-FLU	NIP-PHEN	DIP-PHEN
PFO	Slope	-0.0367	-0.0335	-0.0850	-0.0837
	Intercept	2.0528	2.2118	2.6477	2.7571
	R^2	0.9685	0.9796	0.7113	0.7167
	q_e (mg/g)	7.7900	9.1320	14.1210	15.7540
	k_1 (min^{-1})	0.0367	0.0335	0.0850	0.0837
PSO	Slope	0.1186	0.0976	0.0707	0.0634
	Intercept	1.3651	1.6146	0.0155	0.0154
	R^2	0.9986	0.9981	0.9999	0.9999
	q_e (mg/g)	8.4300	10.2460	14.1410	15.7780
	k_2 ($\text{g mg}^{-1} \text{min}^{-1}$)	0.0103	0.0059	0.3230	0.2610

Table 6. Thermodynamic parameters (ΔH , ΔS , and ΔG) of fluorene and phenanthrene adsorption

Analyte	T (K)	ln K	ΔG (kcal/mol)	ΔH (kcal/mol)	ΔS ($\text{cal mol}^{-1} \text{K}^{-1}$)
Phenanthrene	298	15.9490	-9.4490	-16.1200	-22.0920
	313	15.0503	-9.3650		
	333	13.1135	-8.6810		
Fluorene	298	13.6875	-8.1090	1.1910	31.2070
	313	13.8064	-8.5910		
	333	13.9000	-9.2010		

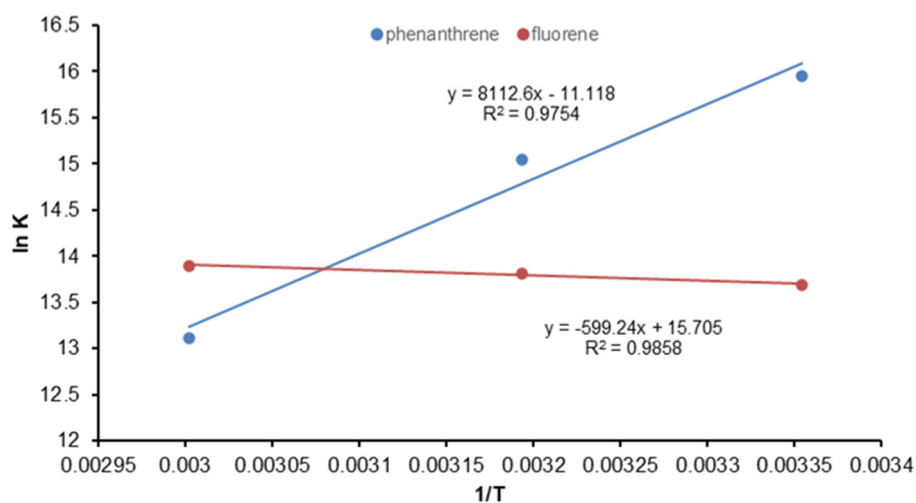


Fig 6. The van't Hoff plot for thermodynamic parameter determination

evidenced by the positive ΔH value ($\Delta H = +1.19$ kcal/mol). This suggests that phenanthrene adsorption is enthalpy-driven, dominated by strong π - π stacking interactions within the imprinted cavities, while fluorene adsorption is entropy-driven, where the gain in configurational freedom of solvent molecules displaced from the binding sites outweighs the relatively weak enthalpic contribution.

In both cases, the ΔG values were negative (-8.11 to -9.45 kcal/mol), confirming that the adsorption process occurred spontaneously at the investigated temperatures. The spontaneity of adsorption decreased slightly with increasing temperature for phenanthrene, consistent with its exothermic nature. In contrast, for fluorene, spontaneity increased with temperature, consistent with an endothermic process.

A notable difference was observed in the entropy change (ΔS). For phenanthrene, ΔS was negative (-22.09 cal mol⁻¹ K⁻¹), indicating a decrease in system disorder upon adsorption. This is consistent with the high planarity of phenanthrene, which allows tight π - π stacking and even dimer formation within the imprinted cavities, restricting molecular freedom. In contrast, fluorene exhibited a positive ΔS ($+31.21$ cal mol⁻¹ K⁻¹), suggesting increased disorder during adsorption. This can be attributed to the non-planar geometry of fluorene, caused by the presence of a C-*sp*³ bridgehead carbon, which reduces π - π stacking propensity and instead relies on weaker hydrophobic and van der Waals interactions.

The less ordered packing of fluorene molecules within the cavities increases entropy, making the process entropy-driven [19-20].

The temperature at which adsorption ceases to be spontaneous can be estimated using the Gibbs free energy equation by setting $\Delta G = 0$. Based on the thermodynamic parameters in Table 6, the adsorption of phenanthrene was calculated to remain spontaneous up to approximately 730 K (457 °C). Above this temperature, ΔG would become positive, indicating non-spontaneous adsorption. In contrast, the adsorption of fluorene was found to reach $\Delta G = 0$ at around 38 K (-235 °C), a temperature far below experimental conditions. As a result, within the studied temperature range (298–333 K), both phenanthrene and fluorene adsorption processes occurred spontaneously. The adsorption of phenanthrene was more favorable at lower temperatures, consistent with its exothermic nature, while the adsorption of fluorene became more favorable at higher temperatures, in line with its endothermic character.

Table 7 presents a comparative analysis of the adsorption capacity between previously reported MIPs and the DIP developed in this study. Traditional sol-gel and bulk MIPs typically exhibited limited adsorption capacities ranging from 0.111 to 1.27 mg/g. In contrast, the present DIP demonstrated markedly superior performance, with adsorption capacities of 12.221 mg/g for fluorene and 16.484 mg/g for phenanthrene. This significant improvement can be attributed not only to the

Table 7. Evaluation of DMIP imprinting factors against selected MIPs for fluorene and phenanthrene

Template	Components	Synthesis approach	Analyte	q _{max} (mg/g)	Ref
16 PAHs (multi template)	PTMS, TEOS	Sol-gel	Fluorene	0.1110	[21]
			Phenanthrene	0.1763	
Pyrene (dummy template)	MAA, 4VP EGDMA	Bulk polymerization	Phenanthrene	0.3700	[22]
16 PAHs (multi template)	MAA, EGDMA	Bulk polymerization	Fluorene	1.2200	[23]
			Phenanthrene	1.2700	
Anthrone (dummy template)	Styrene, EGDMA	Precipitation polymerization	Fluorene	12.2210	Present study
			Phenanthrene	16.4840	

formation of well-defined and highly accessible recognition cavities but also to the use of precipitation polymerization, which produces uniform microspherical particles. The microspherical morphology provides a larger surface area and better exposure of active sites compared to bulk-synthesized MIPs, thereby facilitating more efficient interactions and faster mass transfer with the target analytes.

■ CONCLUSION

A DIP was successfully synthesized using anthrone as a template analog for the selective adsorption of fluorene and phenanthrene. UV-vis titration analyses using the Benesi-Hildebrand and Hill methods established that styrene interacts favorably with the analytes and the dummy template, producing ΔG values ranging from -5.523 to -6.067 kcal/mol for 1:1 binding (Benesi-Hildebrand) and -11.714 to -13.975 kcal/mol for cooperative binding (Hill method). The Hill parameter ($n \approx 1.92$ for anthrone-styrene) indicated that the 1:2 monomer-template complex was thermodynamically preferred and more stable than the 1:1 interaction. These spectroscopic results were further supported by the Job's plot, which showed a clear maximum at a mole fraction consistent with 1:2 stoichiometry. FTIR, TGA, and SEM-BET confirmed successful template removal, adequate thermal stability, and well-formed recognition cavities in the polymer network. Adsorption isotherm studies demonstrated that DIP exhibited significantly higher affinity and capacity than NIP, particularly for phenanthrene due to its more planar aromatic structure, which enhances π - π interactions within the imprinted sites. Adsorption

kinetic studies followed a PSO model, and thermodynamic analysis revealed that phenanthrene adsorption was enthalpy-driven and exothermic, whereas fluorene adsorption was entropy-driven and endothermic. Both adsorption processes were spontaneous, thermodynamic ΔG° values of -9.449 (phenanthrene) and -8.109 kcal/mol (fluorene), thus supporting the coexistence of both 1:1 and 1:2 binding interactions. These findings confirm that anthrone-based DIP provides selective, stable, and energetically favorable binding sites for PAHs, making it a promising material for sensitive and environmentally friendly PAH monitoring.

■ ACKNOWLEDGMENTS

The authors would like to express their sincere gratitude to Institut Teknologi Bandung for the financial support provided through the PPMI KK FMIPA ITB 2024 program (Grant No. 92/IT1.C02/SK-TA/2024) and the Ganesha Talent Award Scholarship (Grant No. 1371/IT1.B04.1/KM.02.00/2020).

■ CONFLICT OF INTEREST

The authors declare no conflicts of interest.

■ AUTHOR CONTRIBUTIONS

Aria Pinandita conducted the experiments and performed the data analysis. Muhammad Ali Zulfikar and Muhammad Bachri Amran supervised and evaluated the experimental and analytical results. Aria Pinandita drafted the original manuscript Nurrahmi Handayani, Muhammad Iqbal, Untung Triadhi, Rusnadi, and Samitha Dewi Djajanti contributed to data

interpretation and manuscript review. All authors read and approved the final version of the manuscript.

■ REFERENCES

- [1] Xie, J., Lan, R., Zhang, L., Yu, J., Liu, X., You, Z., Yang, F., and Lin, T., 2025, Global occurrence, food web transfer, and human health risks of polycyclic aromatic hydrocarbons in biota, *Sci. Total Environ.*, 958, 177969.
- [2] Abdel-Shafy, H.I., and Mansour, M.S.M., 2016, A review on polycyclic aromatic hydrocarbons: Source, environmental impact, effect on human health and remediation, *Egypt. J. Pet.*, 25 (1), 107–123.
- [3] Montano, L., Baldini, G.M., Piscopo, M., Liguori, G., Lombardi, R., Ricciardi, M., Esposito, G., Pinto, G., Fontanarosa, C., Spinelli, M., Palmieri, I., Sofia, D., Brogna, C., Carati, C., Esposito, M., Gallo, P., Amoresano, A., and Motta, O., 2025, Polycyclic aromatic hydrocarbons (PAHs) in the environment: Occupational exposure, health risks and fertility implications, *Toxics*, 13 (3), 151.
- [4] Ncube, S., Madikizela, L., Cukrowska, E., and Chimuka, L., 2018, Recent advances in the adsorbents for isolation of polycyclic aromatic hydrocarbons (PAHs) from environmental sample solutions, *TrAC, Trends Anal. Chem.*, 99, 101–116.
- [5] Jalili, V., Barkhordari, A., and Ghiasvand, A., 2020, Solid-phase microextraction technique for sampling and preconcentration of polycyclic aromatic hydrocarbons: A review, *Microchem. J.*, 157, 104967.
- [6] Ncube, S., Kunene, P., Tavengwa, N.T., Tutu, H., Richards, H., Cukrowska, E., and Chimuka, L., 2017, Synthesis and characterization of a molecularly imprinted polymer for the isolation of the 16 US-EPA priority polycyclic aromatic hydrocarbons (PAHs) in solution, *J. Environ. Manage.*, 199, 192–200.
- [7] Azizi, A., Shahhoseini, F., and Bottaro, C.S., 2020, Magnetic molecularly imprinted polymers prepared by reversible addition fragmentation chain transfer polymerization for dispersive solid phase extraction of polycyclic aromatic hydrocarbons in water, *J. Chromatogr. A*, 1610, 460534.
- [8] Chauhan, A., Bhatia, T., Singh, A., Saxena, P.N., Kesavchandran, C., and Mudiam, M.K.R., 2015, Application of nano-sized multi-template imprinted polymer for simultaneous extraction of polycyclic aromatic hydrocarbon metabolites in urine samples followed by ultra-high performance liquid chromatographic analysis, *J. Chromatogr. B*, 985, 110–118.
- [9] Kibechu, R.W., Sampath, S., Mamba, B.B., and Msagati, T.A.M., 2017, Graphene-based molecularly imprinted polymer for separation and pre-concentration of trace polycyclic aromatic hydrocarbons in environmental water samples, *J. Appl. Polym. Sci.*, 134 (37), 45300.
- [10] Egli, S.N., Butler, E.D., and Bottaro, C.S., 2015, Selective extraction of light polycyclic aromatic hydrocarbons in environmental water samples with pseudo-template thin-film molecularly imprinted polymers, *Anal. Methods*, 7 (5), 2028–2035.
- [11] Abdella, A.A., and Ulber, R., 2025, Dummy-template molecularly imprinted polymers as an approach for improved efficiency for analytical applications: A mini review, *Microchem. J.*, 209, 112768.
- [12] Fu, X., Wang, X., Xia, Z., and Huang, Y., 2022, Preparation of dummy molecularly imprinted polymers for selective extraction of aromatic amine genotoxic impurities, *J. Chromatogr. A*, 1685, 463617.
- [13] Bagheri, A.R., Arabi, M., Ghaedi, M., Ostovan, A., Wang, X., Li, J., and Chen, L., 2019, Dummy molecularly imprinted polymers based on a green synthesis strategy for magnetic solid-phase extraction of acrylamide in food samples, *Talanta*, 195, 390–400.
- [14] Yuan, Y., Yuan, X., Hang, Q., Zheng, R., Lin, L., Zhao, L., and Xiong, Z., 2021, Dummy molecularly imprinted membranes based on an eco-friendly synthesis approach for recognition and extraction of enrofloxacin and ciprofloxacin in egg samples, *J. Chromatogr. A*, 1653, 462411.
- [15] Zhang, Y., Li, S., Gu, Y., Zhang, J., Yue, Z., Ouyang, L., and Zhao, F., 2023, Dummy template-based

- molecularly imprinted membrane coating for rapid analysis of malachite green and its metabolic intermediates in shrimp and fish, *Molecules*, 28 (1), 310.
- [16] Sheng, T.P., Fan, X.X., Zheng, G.Z., Dai, F.R., and Chen, Z.N., 2020, Cooperative binding and stepwise encapsulation of drug molecules by sulfonylcalixarene-based metal-organic supercontainers, *Molecules*, 25 (11), 2656.
- [17] Khatibi, A.D., Mahvi, A.H., Mengelizadeh, N., and Balarak, D., 2021, Adsorption-desorption of tetracycline onto molecularly imprinted polymer: Isotherm, kinetics, and thermodynamics studies, *Desalin. Water Treat.*, 230, 240–251.
- [18] Wnuczek, K., Podkościelna, B., Sobiesiak, M., Szajnecki, Ł., and Goliszek, M., 2020, Synthesis and modification by carbonization of styrene-ethylene glycol dimethacrylate-lignin sorbents and their sorption of acetylsalicylic acid, *Materials*, 13 (7), 1761.
- [19] Lamichhane, S., Bal Krishna, K.C., and Sarukkalige, R., 2016, Polycyclic aromatic hydrocarbons (PAHs) removal by sorption: A review, *Chemosphere*, 148, 336–353.
- [20] Said, T.O., Al-Farhan, B.S., El-Ghamdi, S.A., and Awwad, N., 2024, Biosorbent treatment of fluorene using activated carbon derived from the pyrolysis process of date pit wastes, *Sci. Rep.*, 14 (1), 22039.
- [21] Song, X., Li, J., Xu, S., Ying, R., Ma, J., Liao, C., Liu, D., Yu, J., and Chen, L., 2012, Determination of 16 polycyclic aromatic hydrocarbons in seawater using molecularly imprinted solid-phase extraction coupled with gas chromatography-mass spectrometry, *Talanta*, 99, 75–82.
- [22] Xie, J., Cai, C., Lai, S., Yang, L., Luo, L., Yang, H., Chen, Y., and Chen, X., 2013, Synthesis and application of a molecularly imprinted polymer as a filter to reduce polycyclic aromatic hydrocarbon levels in mainstream cigarette smoke, *React. Funct. Polym.*, 73 (12), 1606–1611.
- [23] Krupadam, R.J., Bhagat, B., Wate, S.R., Bodhe, G.L., Sellergren, B., and Anjaneyulu, Y., 2009, Fluorescence spectrophotometer analysis of polycyclic aromatic hydrocarbons in environmental samples based on solid phase extraction using molecularly imprinted polymer, *Environ. Sci. Technol.*, 43 (8), 2871–2877.